ENHANCING SEISMIC RESOLUTION BASED ON U-NET DEEP LEARNING NETWORK

ZEYU LI[1,2] , GUOQUAN WANG[1,2] , CHENGHONG ZHU[2,3,4] and SHUANGQUAN CHEN[1]*

[1] *College of Geophysics, China University of Petroleum (Beijing), 102249 Beijing, P.R.China. * chensq@cup.edu.cn*
[2] *State Key Laboratory of Shale Oil and Gas Enrichment Mechanisms and Effective Development, 100083 Beijing, P.R. China.*
[3] *Sinopec Key Laboratory of Seismic Elastic Wave Technology, 100083 Beijing, P.R.China.*
[4] *Sinopec Petroleum Exploration and Production Research Institute, 100083 Beijing, P.R. China.*

ABSTRACT

Li, Z.Y, Wang, G.Q., Zhu, C.H. and Chen, S.Q., 2023. Enhancing seismic resolution based on U-Net deep learning network. *Journal of Seismic Exploration*, 32: 315-336.

Deep and ultra-deep reservoirs, unconventional hydrocarbons, and other complex reservoirs are being developed for oil and gas exploration. High-resolution with high signal-to-noise ratio seismic data is required for accurate reservoir description. Therefore, high-resolution seismic data processing is a challenging and important endeavor. The conventional high-resolution processing techniques, such as inverse Q-filtering technique based on the stratum attenuation model and deconvolution methods, are nearly model-dependent. Deep learning method based on image processing has been widely used in seismic data processing and inversion in recent years, which is a data-driven method and has powerful abilities to extract data features. In this paper, we rebuild a deep learning network based on U-net network and proposed a high-resolution seismic data processing method and workflow. In the network, we utilized *ResPath* structure instead of the straightforward skip connection in the conventional Res-Unet, and employed a combination loss function by using the mean absolute error and multiscale structural similarity. Moreover, by introducing pre-training strategy into the processing workflow, the proposed network can reduce the loss of low-frequency components and perceive low-frequency information. Synthetic and real field seismic data are used to validate the network, the trained model by using pre-training strategy can better maintain the low-frequency components of the original data and recover the high-frequency components, and the signal-to-noise ratio and resolution of seismic data have both been significantly enhanced.

KEY WORDS: U-net, deep learning, pre-training strategy, seismic resolution, data-driven.

INTRODUCTION

By receiving reflection wave information of the underlying strata at the surface, seismic exploration can identify the underground geological structure and physical properties. When seismic waves propagate into the underground medium, various factors including spherical diffusion and absorption attenuation will lead to the energy attenuation and velocity dispersion, which induces weak energy and phase delay at the large offset and deep record, and the overall continuity of seismic events becomes worse. Further, it is challenging to effectively describe and interpret reservoirs with thin reservoirs and small faults. Therefore, it is necessary typically that processing the seismic data to improve the resolution due to the rising demand for oil and gas exploration and development. High-resolution processed seismic data contains abundant geological information, which is more conducive to seismic interpretation, reservoir prediction and attribute analysis. Consequently, a number of model-based techniques for enhancing seismic resolution have been proposed, including the conventional deconvolution (Robinson et al., 1967), non-stationary seismic signal convolution model technology (Margrave et al., 2011), absorption attenuation compensation technology based on one-dimensional continuous wavelet transform (Braga and Moraes, 2013), low frequency broadening technology based on compressed sensing algorithm (Zhang et al., 2015), spectral bluing (Kazemeini et al., 2010), spectral whitening method based on Hilbert-Huang transform (Yan et al., 2018), wavelet compression method that utilizes the scale characteristic in the Fourier transform (Chen and Wang, 2018) and shaping regularization inverse Q-filtering (Chen et al., 2018). Deconvolution and inverse Q-filtering are typically thought of as model-driven techniques, while amplitude compensation and phase correction of seismic data utilize the convolution model and absorption attenuation model's presumptions. However, further research is necessary to determine whether the theoretical model is appropriate for actual subsurface reflection. In recent years, with the improvement of GPU computing power and the rapid development of deep learning theory, many tasks that were costly and time-consuming have been effectively solved with the help of data-driven methods. The application of deep learning in the field of geophysics is also growing rapidly, some progress has achieved in seismic data denoising (Yu et al., 2019), fault identification (Wu et al., 2019), river channel detection (Gao et al., 2021) and seismic lithofacies classification (Jervis et al., 2021).

The fundamental principle of deep learning is to build a multi-layer nonlinear transformation method to transform the representation of samples in the original space into a new feature space. Consider a multi-layer neural network as an illustration, inherent patterns and feature representation of the sample data can be learned by each layer of the neural network, and through nonlinear mapping, simple and primary features can be transformed into higher dimensional and more abstract features. However, the higher dimensional features will have more semantic information, which will magnify the information critical for discrimination and suppress the irrelevant information in the input data. With enough of these layers, complex patterns in

data can be identified and used to solve complex problems in unstructured data processing (LeCun et al., 2015). The network architecture of deep learning is made up of the stacking of layers, which is essential for accuracy. Typical network architectures include VGGnet, U-net, and Alexnet, etc. Among them, U-net is proposed by Ronneberger (2015), which is developed from full convolutional neural network (Long et al., 2015). At present, the common network structures for image super resolution processing include SRCNN (Dong et al., 2015) and SRGAN (Ledig et al., 2017), etc. However, the definition of resolution in pictures is simply restricted to the clarity of the images, which is different from the definition of resolution in geophysics. To meet the demands of high precision processing of actual data, the latter must build new techniques.

It is required to increase the high frequency signal-to-noise ratio (SNR) and frequency band width to enhance the resolution of seismic data. The broadening of the frequency band by using deep learning is an effective method to improve the resolution. The model must be fully trained in this method, which is entirely data driven and does not require the seismic wavelet assumption. Based on the original seismic data, high-resolution processing results can be acquired directly. Canning et al. (2017) used multi-layer perceptron to effectively broaden the spectrum of seismic data and improve the resolution of seismic data. Halpert (2018), Picetti et al. (2018) and Oliveira et al. (2019) simulated a denser geometric acquisition structure and improved the resolution of seismic data by using a generated adversarial network. Yuan et al. (2019) proposed a seismic profile reconstruction method based on convolutional neural network combined with super resolution reconstruction technology. Deng et al. (2020) proposed a combination of dual convolution and attention mechanism at the top of the network to extract multi-scale features of seismic data and improve the seismic resolution. Li et al. (2020) combined MS-SSIM loss and MAE loss as a new loss function to effectively improve the details of the seismic profile after resolution improvement. Sun (2021) trained the end-to-end U-Net, which significantly improved the resolution of seismic data; Choi et al. (2021) developed a spectrum enhancement technology based on machine learning, which effectively improved the accuracy of signals after frequency enhancement through the fusion of prior information. There are still certain issues even though these studies can make up for the original data's high frequency. Although the resolution is visually improved by simply mapping low-frequency seismic data to high-frequency seismic data using deep learning networks, the low-frequency features of the original signal are lost in the processed data, which is detrimental to the improvement of data quality (Li, 1994). On the other hand, inappropriate loss function selection will produce data with artifacts (Li et al., 2020). These negative effects will interfere later seismic interpretation.

Some recent convolutional neural networks try to address common deep learning issues including vanishing gradient, expanding gradient, and overfitting by introducing new modules, while retaining the core idea of the U-net. The proposal of *Res-Unet* (Xiao et al., 2018) aims to find a balance point between the linear transformation and the nonlinear transformation.

Considering the structural complexity of seismic data, the semantic information lost by pooling operation will have some adverse effects on the prediction process, the *ResPath* (Ibtehaz et al., 2019) is used to process the data before data fusion, which makes learning easier.

In this paper, by integrating a *ReSPath into Res-Unet and adding new training strategies to network training,* we successfully improve the network's information mining performance of seismic data and increase its capacity to perceive low-frequency components of seismic data. Our approach eliminates output result artifacts while resolving the issue of low frequency component loss in deep learning seismic data. Finally, our method is tested using synthetic and field data.

METHODOLOGY

Network architecture

To improve the resolution of seismic data, we employ a deep learning network. The deep learning network aims to account for the relationship between low-resolution sample and high-resolution label based on data-driven idea,

$$D_{\mathrm{H}} = \mathrm{Net}(\mathbf{q}, D_{\mathrm{L}}) \quad , \tag{1}$$

where Net represents the network architecture of deep learning network, D_L and D_H represent low-resolution seismic sample and high-resolution seismic label respectively, and $\theta = \{W, b\}$ contains network parameters, weight W and bias b. In order to ensure that the data generated by the model closely resembles the real data and creates the best mapping relationship between D_L and D_H, network training primarily uses the back propagation algorithm to update network parameters and reduce the loss function value between the network prediction data and the real data.

The U-net architecture used in our method is illustrated in Fig. 1, which adopts the Res-Unet network structure (Xiao et al., 2018) and introduces the *ResPath* structure from MultiResUnet (Ibtehaz et al., 2019). The network can be divided into three different sections based on its actual purpose. The first section is the trunk feature extraction part, which is a combination of convolutional layer (3×3), batch normalization layer, residual module, activation function and max-pooling layer (2×2). Through this section, we can obtain five preliminary effective feature layers, each of which has a channel number of 64, 128, 256, 512, and 1024. The second section contains high and low dimensional feature transmission part. The skip connection in the conventional U-net is replaced with a *ResPath*, which makes it simpler for the model to learn the feature information required to enhance resolution. The number of four *ResPaths* from the shallow layer to the deep layer of the revised network model is specified as 4, 3, 2, and 1, correspondingly, since the data features after down sampling will decrease as the

network is deepened. The third section is the feature fusion part. We connect the data features obtained via the second section's residual path to the outputs from transposed convolution, and then proceed through the convolution layer (3×3), batch normalization, and residual modules successively, obtaining an output data that incorporates all characteristics.
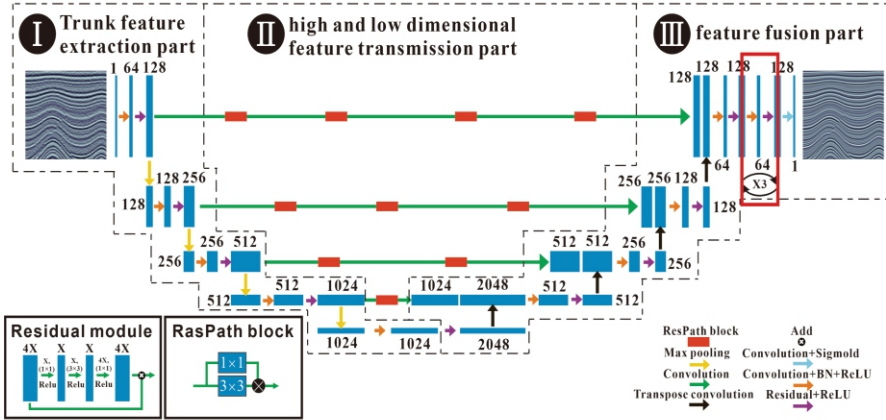

Fig. 1. U-Net architecture with *ResPath*. There are three parts in the network, part-I trunk feature extraction, part-II high and low dimensional feature transmission and part-III feature fusion part.

The purpose of adopting Res-Unet architecture is to introduce nonlinear processing through the residual module. The residual module, which is seen in the lower left corner of Fig. 1, uses a shortcut to transmit shallow layer feature information to the deeper layer more quickly while avoiding gradient disappearing and gradient exploding. Even if the network has numerous layers, the presence of this module can still minimize training loss values steadily and constantly, solve training challenges brought on by the depth of the network, and guarantee that the deep learning network's performance won't decline (He et al., 2016). In addition, considering that the network will obtain different dimensional feature information after down- and up-sampling, direct splicing would also negatively affect network training, but the nonlinear operation in the *ResPath* can narrow the semantic gap between the two (Ibtehaz et al., 2019). However, deep learning suffers a more difficult challenge with generalization than fitting. The overfitting issue must be resolved because the training set is unable to cover all cases. Ioffe et al. (2015) proposed batch normalization, which enables all samples in a batch to be associated together. In this situation, a model is somewhat protected from overfitting because it depends on other samples in the same batch in addition to the sample itself. The specific form of batch normalization is

$$y_i = \gamma \frac{x_i - \mu}{\sqrt{\sigma^2 + \varepsilon}} + \beta , \tag{2}$$

where μ and σ are respectively the mean value and variance of the i-th layer, x_i are the input data of the i-th layer, and ε is a constant to ensure the stability of the operation, γ and β are scale and offset, which can prevent the normalization from destroying the original feature distribution of the data. To address the overfitting issue during network training and assure the model's generalization ability, this method is used in this research to introduce randomness into the network.

Loss function

The loss function is intended to measure the difference between the output data of the network and the label data during training. The direction of optimization is controlled by the loss function value, and its general form is as follows:

$$L = f(y_{true}, y_{pred}) , \tag{3}$$

where y_{true} and y_{pred} are label data and network output data respectively, and f is the function to evaluate the difference between them. The forward propagation algorithm calculates the loss function value for each iteration, and the back-propagation algorithm uses the obtained results to solve the partial derivative for each layer. The loss function will eventually approach the minimum by altering the parameters of each layer. The output results of the current network will be directly impacted by the loss function selection. MAE index is generally used to quantify the data difference in regression problems. MAE is defined as

$$L^{MAE}(y_{true}, y_{pred}) = \frac{1}{m} \sum_{i=1}^{m} | y_i - y_i' | \tag{4}$$

where y_i and y_i' are the i-th elements of label data and network output data respectively, and m is the number of elements in the data. However, if MAE is the only loss function used, the output of this network will lose the seismic data's longitudinal variation characteristics and will not consider the features of microgeological structures like thin layers and tiny faults. So, as a loss function, we employ the MS-SSIM function. The MS-SSIM function is more sensitive to the identification of microgeological features in space when local resolution is considered in addition.

The MS-SSIM function system is shown in Fig. 2. Multi-scale means that data indicators need to be measured at different scales. The original seismic data is defined as X, and the seismic data after 4 subsampling is defined as X5.
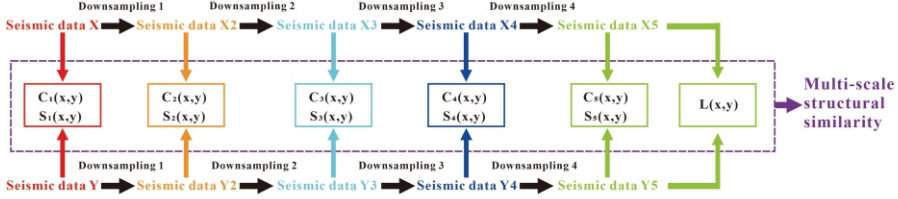

Fig. 2. Structure of multi-scale structure similarity loss function.

The MS-SSIM function uses filter operators of different sized to expand the receptive field, catching statistical characteristics on various scales while preserving consistency with subjective perception. The definition of the function is showed as follows:

$$f(x,y) = [l(x,y)]^{\alpha} \prod_{j=1}^{5} [c_j(x,y)]^{\beta_j} [s_j(x,y)]^{\gamma_j} , \qquad (5)$$

where x and y represent the data following the down sampling of high-frequency labels and network output separately. α, β_j and γ_j are used to adjust the relative importance of different similarity degrees. In this paper, we set $\alpha = 0.1333$, $\beta_j = \gamma_j =$ [0.0448, 0.2856, 0.3001, 0.2363, 0.1333]. The three measures between x and y are denoted by the parameters $c_j(x,y)$, $s_j(x,y)$, and $l(x,y)$, which stand for the wavelet's width, structure, and amplitude in seismic data. These are their definitions:

$$c(x,y) = \frac{2\sigma_x \sigma_y + C_1}{\sigma_x^2 + \sigma_y^2 + C_1} , \qquad (6)$$

$$s(x,y) = \frac{\sigma_{xy} + C_2}{\sigma_x \sigma_y + C_2} , \qquad (7)$$

$$l(x,y) = \frac{2\mu_x \mu_y + C_3}{\mu_x^2 + \mu_y^2 + C_3} , \qquad (8)$$

where μ and σ are the mean and standard deviation of the seismic data respectively, and σ_{xy} are the covariance between x and y. Three constants, C_1, C_2, and C_3 ensure the stability of the operation. It must be noted that covariance σ_{xy} can be of negative value which may lead $s(x,y)$ to be of negative number. To ensure that the range of MS-SSIM value is 0 to 1, we need to modify it as a loss function. We can achieve the goal with a simple transformation and the transformation is defined as:

$$L^{MS-SSIM}(y_{true}, y_{pred}) = 1 - (1 + f(y_{true}, y_{pred}))/2 . \qquad (9)$$

In order to improve the perception of recovered high-resolution seismic data, we combine the MAE loss and MS-SSIM loss as a new loss function defined as:

$$L^{\text{mix}} = \alpha L^{MAE} + (1 - \alpha) L^{MS-SSIM} , \tag{10}$$

where α is the weight of MAE function in the mixed loss function. With reference to the experiments of Zhao et al. (2016), we set different weight values for the loss function and compared the training results of the network with different weights to evaluate the effectiveness of the mixed loss function in enhancing the resolution of seismic data. Table 1 displays the value of the PSNR (peak signal-to-noise ratio) during the training process with different weights. When α = 1 and 0.16, it demonstrates that our network has attained good performance. Fig. 3's comparative findings include the model output at α values of 1 and 0.16, where α = 1 represents training outcomes when only the MAE function is used as a loss function. When compared to the original data, the MAE output (Fig. 3c), which is displayed close to the red rectangles, indicates that the seismic events in the upper part of the seismic data appear to be artifacts and that the resolution of the strata at the bottom of the data was not significantly improved (Fig. 3a). The recovered seismic data appears more realistic when α = 0.16, which is an appropriate parameter choice, when comparing the output of mixed loss of various weights.

Table 1. PSNR in the training process with different loss function weights.

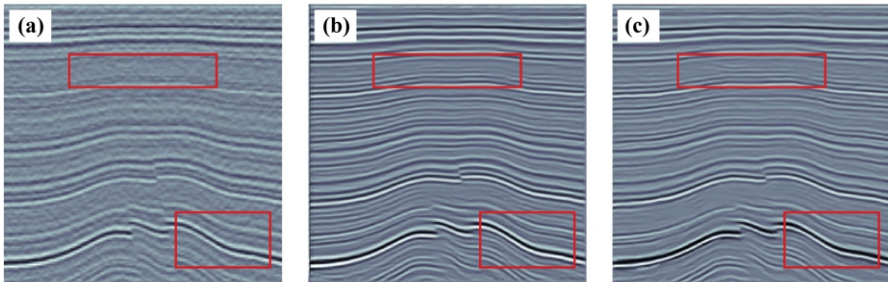| α	1	0.8	0.6	0.4	0.2	0.16	0.1	0
PSNR	22.5126	22.0756	21.1443	21.9426	21.914	22.4532	22.116	21.6869

Fig. 3. Comparison of high-resolution labels with the different loss function weight factor α. (a) original seismic data sample; (b)-(c) α are 0.16 and 1, respectively. The red rectangles represent the difference.

NETWORK TRAINING

Data preparation

There must be many samples and corresponding labels for the deep learning network to be trained. It has been found that if we use field seismic data as the training set in the training process, the entire process will be influenced by irrelevant factors such noise and amplitude attenuation, which will lead in the network's entire mapping relationship being unclear. Wu et al. (2019) proposed to train the network with synthetic data in fault identification and applied it in field data, greatly improving the accuracy of fault identification. Wherefore, we use reflection coefficient sequences to convolve with seismic wavelet of various frequency band widths to build low-resolution sample and high-resolution label. First, we decide to employ Ricker wavelet to make low-resolution sample. The low-frequency and high-frequency component information should be fully retained for high-resolution labels. We utilize wide-band wavelet to create high-resolution labels because its main lobe is relatively narrow, its side lobe amplitude is small, its waveform is simple, and its peak frequency of the amplitude spectrum is relatively low for the same main lobe width (Yu, 1996). The specific forms of zero-phase Ricker wavelet W_L and wide-band wavelet W_H are:

$$\begin{cases} W_L(t) = (1 - 2(\pi f_p t)^2)e^{-(\pi f_p t)^2} \\ W_H(t) = \dfrac{1}{q-p}\int_p^q [1 - 2(\pi f t)^2]e^{-(\pi f t)^2}\, df \end{cases}, \qquad (11)$$

where t is the time, f_p is the peak frequency of zero-phase Ricker wavelet, p and q are the lower and upper cut-off frequency of wide-band wavelet respectively. In our study, we used 30 Hz for the peak frequency of Ricker wavelet, 10 Hz for the lower cut-off frequency of the wide-band wavelet, and 80 Hz for the upper cut-off frequency. We added random noise with a signal to noise ratio (SNR) of 6.5 to the low-resolution sample to bring the sample closer to the real data. Considering that the convolutional kernel can only learn the structure reflected by the samples and labels, and that the patch input into the network should contain enough layers and fault information, as well as avoid occupying too much memory, we randomly clipped the samples and labels to 256×256 and input them into the network for training. We produced 500 pairs of data sets, 450 of which were used as training sets and 50 as validation sets. Fig. 4 displays the generated data. The seismic events of high-resolution label are more numerous and thinner than those of low-resolution sample.
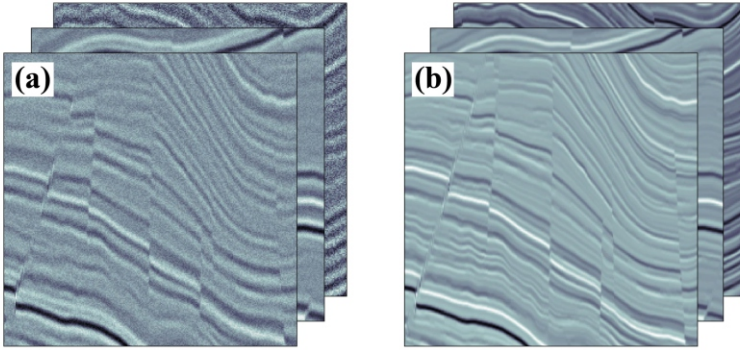
Fig. 4. (a) Low-resolution samples; (b) high-resolution label.

Pre-training

Pre-training may significantly increase the network's performance and effectiveness for data mining in deep learning training. The pre-trained model is trained by the enormous data first, and then it is applied to the task. Pre-training is a popular and efficient method for transferring information from target tasks to related tasks. This method can provide the model a high-quality initialization, enhancing the model's performance. Strong portability exists for the spatial features that were learnt from the pre-training network. Considering that seismic data with different main frequencies have similar spatial structure characteristics and have portability, we used the pre-training strategy to carry out the resolution improvement task.

While the layer towards the top of the model extracts the more abstract feature map, the layer near the bottom extracts the local, more generic feature map. To preserve the shallow spatial features in the reuse model and account for some differences between the new and the original data sets, we reset some parameters at the top of the pre-training network. We slightly modified the more abstract representation to make the network more applicable to the issue at hand. Specifically, we pre-trained the network using the low-resolution samples and the corresponding high-resolution labels provided as open-source (Fig. 5) by Li et al. (2020), using 3000 pairs as training sets and 200 pairs as validation sets. We then used the data we generated (Fig. 4) to re-train the network, using 450 pairs as training sets and 50 pairs as validation sets.

The amplitude of seismic data obtained in the same region may fluctuate noticeably depending on the collecting conditions, geological structure, and burial depth. The data that is directly processed is evidently inconsistent with the features of seismic data because the ReLU activation function used after each convolution layer will set the negative elements to zero. Therefore, we should first preprocess samples and labels before training, that is, normalize all the seismic data to be trained, so that the training data is closer

to the relative amplitude relationship between the original data. The form of normalization processing is as follows:

$$x* = \frac{x - x_{\min}}{x_{\max} - x_{\min}} \quad , \tag{12}$$

where $x*$ is the normalized value of seismic data, x is the real value of each point in the seismic data, and $x_{\max}$ and $x_{\min}$ are the maximum and minimum values of each input seismic data respectively. The normalized data are all in the range of [0,1], which avoids the influence of the difference in seismic amplitude of different data sets. To further boost the diversity of the data set, we also added a simple geometric manipulation which required randomly flipping pairs of data. The network test environment was NVIDIA GeForce RTX 2080Ti GPU and the memory was 11GB. In the process of configuring the compiler, we used the Adam optimizer and set the parameter $\beta_1 = 0.9$, $\beta_2 = 0.999$, $\varepsilon = 10^{-8}$. At the same time, the loss function is a weighted combination of MAE loss and MS-SSIM loss with $\alpha = 0.16$, and PSNR is used as the metrics function of the model. The metrics function is only used to evaluate the network capability and will not participate in the adjustment of network parameters in the process of back propagation.
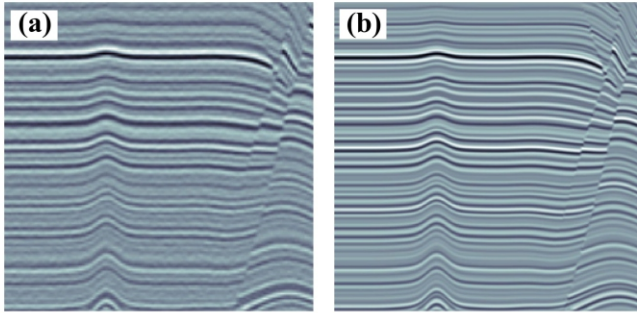

Fig. 5. Open source high and low frequency data by Li et al. (2020).

First of all, we trained the network for the first time using open-source data by Li et al. (2020). We set the parameter batch size = 64, learning rate = 0.001, and train our network over 50 epochs. After about 30 iterations, the network has converged. The validation set's loss function achieved 0.022 and the PSNR hit 23.7 after 50 iterations. It took roughly 30 minutes to complete the process. The loss function and PSNR curve are both replaced with an exponential moving average for interpretability. In Fig. 6 below, the training's loss function and metrics function curves are displayed.
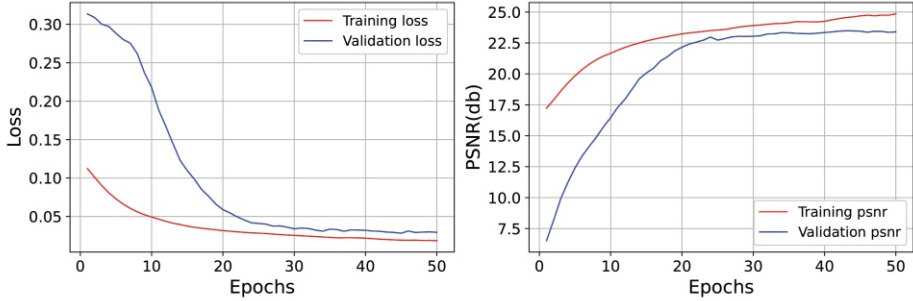
Fig. 6. Loss and metrics curves during network pre-training.

After pre-training the network, we altered the parameters of the three residual modules at the top of the network (the section highlighted in red in Fig. 1) to an updateable state to obtain a new network with improved perception capabilities for certain frequencies. And then, we employ 500 pairs of seismic data obtained using a Ricker wavelet and wide band wavelet as samples and labels, of which 450 pairs are used to train the new network and the remaining 50 pairs to validate it. In a new round of training, considering the network already has a certain frequency enhancing capability, the learning rate parameter of Adam optimizer is set as 0.0001. At the same time, we set the epoch parameter to 100 and the other parameters remain unchanged. The ability of the new network changes with the number of iterations, and its training curve is shown in Fig. 7. The network performs better on the validation sets in the early stages of training since there are fewer number of validations set and their distribution is uneven. As network training times arise, the network will eventually converge after around 50 iterations, at which time the loss value will ultimately reach 0.072 and the PSNR will reach 22.7, taking about 10 minutes. We now think that the network has picked up a new mapping mode.
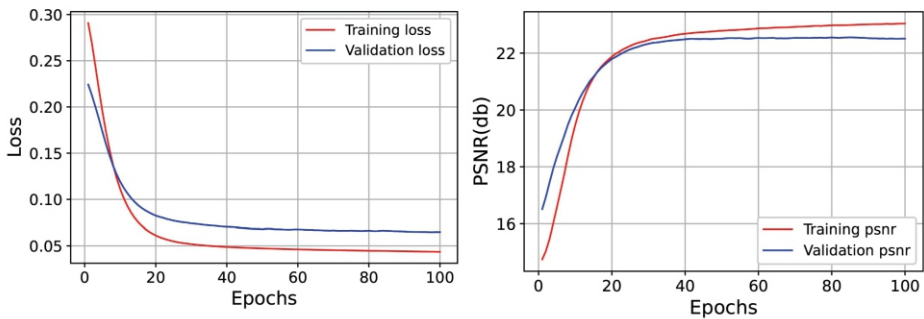

Fig. 7. Loss and metrics curves for network training.

We randomly select a seismic profile in the validation set for frequency enhancement (Fig. 8). Fig. 8a shows the low-resolution data with noise, Fig. 8b shows the seismic data produced by the model, and Fig. 8c shows the high-resolution label corresponding to a. Compared with Fig. 8a, Fig. 8b has enhanced some small layer features, as shown in the two red rectangles in the figure. Even in low-resolution seismic data, there are some traces that cannot be discriminated by the naked eye between the two layers; however, the network can effectively recover these thin layers. Additionally, the network obviously has a denoising effect.
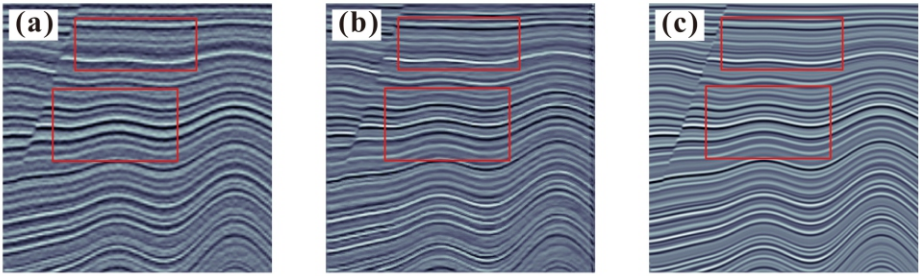
Fig. 8. Comparison test in a validation set.   (a) Low-frequency data;   (b) Model output data;   (c) High-frequency label

Finally, the mean absolute error, mean square error and multi-scale structural similarity between a, b and c were calculated. Table 2 demonstrates that b is located between values a and c in various numerical representations. Compared with the original data a and c, b and c are more similar.

Table 2. Numerical comparison between a, b and c.

	a and c	a and b	b and c
MAE	17.410965	13.707064	9.743504
MSE	500.5979004	307.0289307	177.3246453
MS-SSIM	0.876802908	0.871912015	0.965872094

DATA APPLICATION

Synthetic data example

To verify the improvement of pre-training on the overall performance of the network, the model was first used for synthetic data and compared it with the effect of the network trained only once using our data. Firstly, we use Ricker wavelet with a peak frequency of 40 Hz to make synthetic data and add gaussian noise with a signal-to-noise ratio of 6.5 to simulate the real strata. Because the model only handles data within the range [0,1], we must first normalize the synthetic data. In addition, the network was downsampled for four times, so the length of data input to the network must be a multiple of 16. We set the size of the synthetic data to 1200×800.
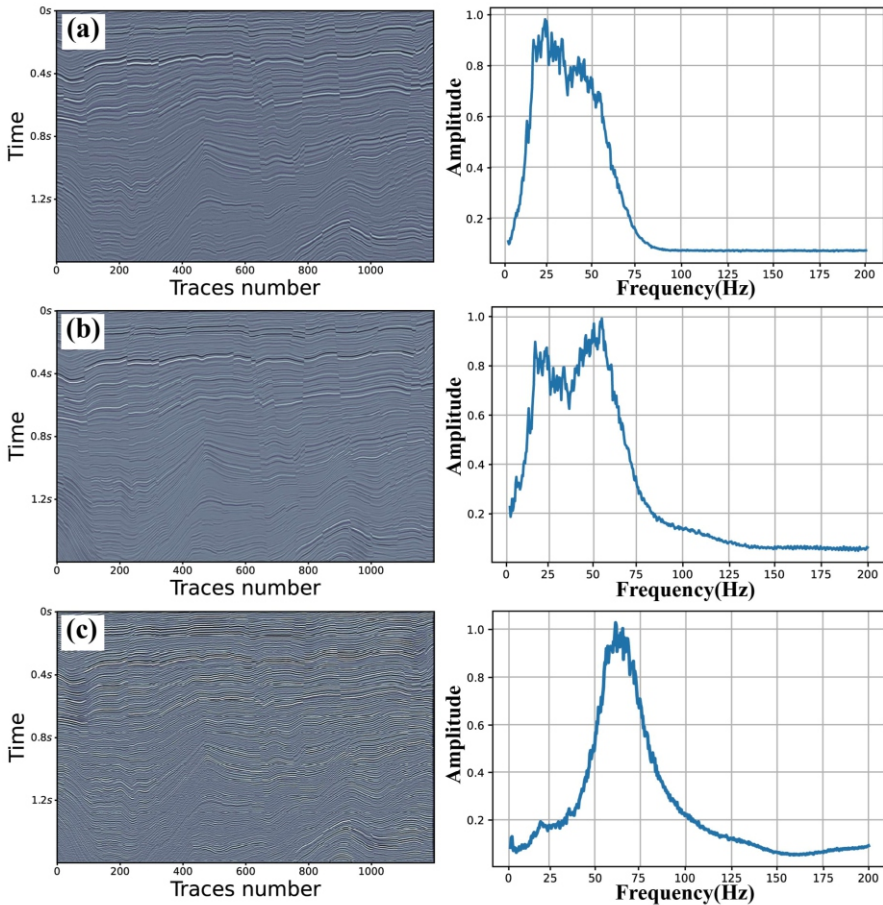
Fig. 9. Comparison of network effect of pre-training or not. (a) Original data; (b) Model output of the pre-training network; (c) model output of the network trained only once using our data.

We put the synthetic data into both the network trained only once using our data and the network trained by the method in this paper. It is discovered that the pre-training strategy may enhance the performance and effectiveness of the network for data mining by comparing the output results of the two ways. The main frequency component of the synthetic data is around 25 Hz, as seen in Fig. 9a. The high-resolution data output by the network is shown in Fig. 9b. Besides the 25 Hz portion, the 60 Hz portion of the main frequency component is also mined; Fig. 9b illustrates this trend in a clear example. The output of the model trained only once using our data is displayed in Fig. 9c. The main frequency component is enhanced to roughly 60 Hz, which has a positive effect on the profile, but the bandwidth is narrowed and the low frequency component is lost. Importantly, the enhanced frequency is unwarranted.

Fig. 10a shows an example where a low-resolution seismic data is directly using the synthetic data showed in Fig. 9a. Feeding this native data into our trained CNN model, we obtain an improved seismic data shown in Fig. 10b. From the overall effect, the seismic data has thinner layer and its longitudinal resolution is improved effectively after network processing. At the same time, the layers are smoother and cleaner, and its fault structure is obviously retained. The zoomed-in views of the synthetic data and the model's output data may be seen in the red rectangles, which are shown in more detail. The model recovers the structures shown by the arrows, which represent thin layers that are blurred on the low-resolution seismic data or regions with modest amplitude fluctuations. In addition, the model effectively removes the noise from the original data.
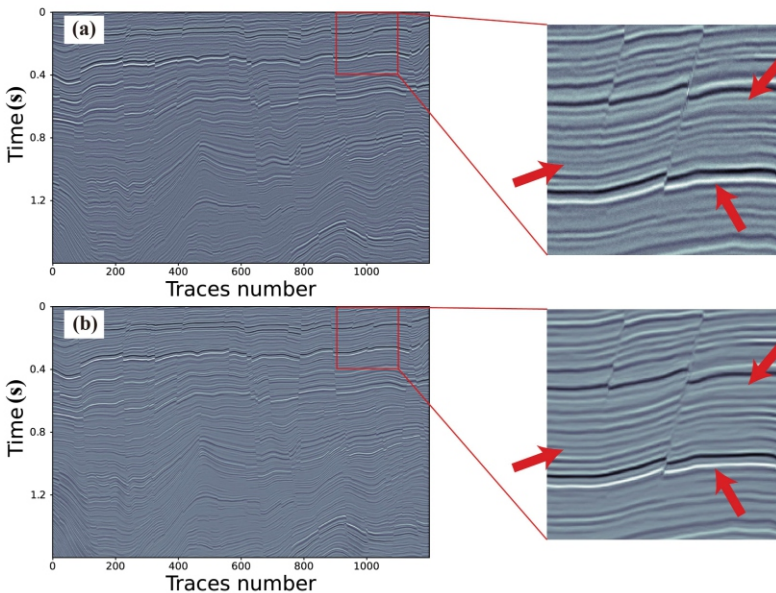

Fig. 10. Comparison test in a synthetic data. (a) Original data and (b) the output of the model.

Spectrum analysis of the original data and the model output (Fig. 10) is illustrated in Fig. 11. The blue and red curves reflect the amplitude spectrum of the original data and the amplitude spectrum of the model output data, respectively, and the green arrows indicate the source of the variation in the high-frequency component. It is clear from spectrum analysis that the model significantly enhances the upper cut-off frequency, greatly improves the main frequency of seismic data, and notably widens the frequency band. The main frequency of seismic data is enhanced from 35 Hz to roughly 41 Hz while the low-frequency component is maintained, enhancing the longitudinal resolution of the data.
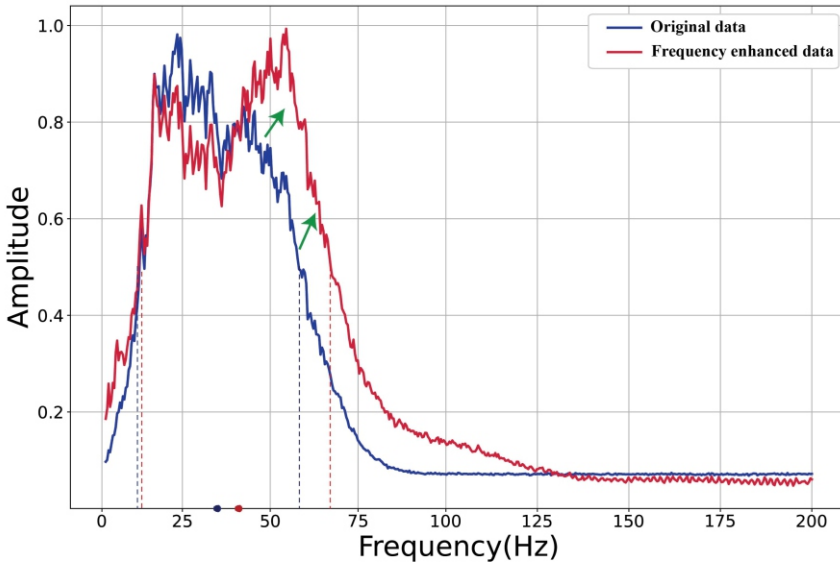

Fig. 11. Spectrum analysis of the synthetic seismic data.

FIELD DATA APPLICATION

We use the field seismic data (Fig. 12) of a work area as the data to be trained to test the network's processing effect on the field data.

The work area has 251 Xlines and 21 Inlines with a 2 ms time sampling rate. We used the Fourier transform to analyze it, and the spectrum ranges from 17 to 56 Hz. First, we randomly extracted a 2D section with a size of 736×640 from the field data and normalized it. Once the field data is entered the model, enhanced resolution seismic data can be obtained in a few milliseconds. Fig. 13 illustrates the observation of the model's output data, which reveals the identification of hidden strata in seismic events, a significant improvement in the resolution of the seismic data, and a large reduction in noise.
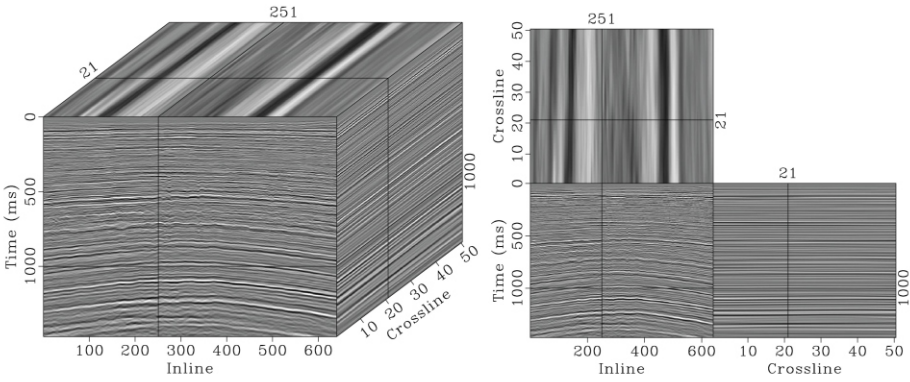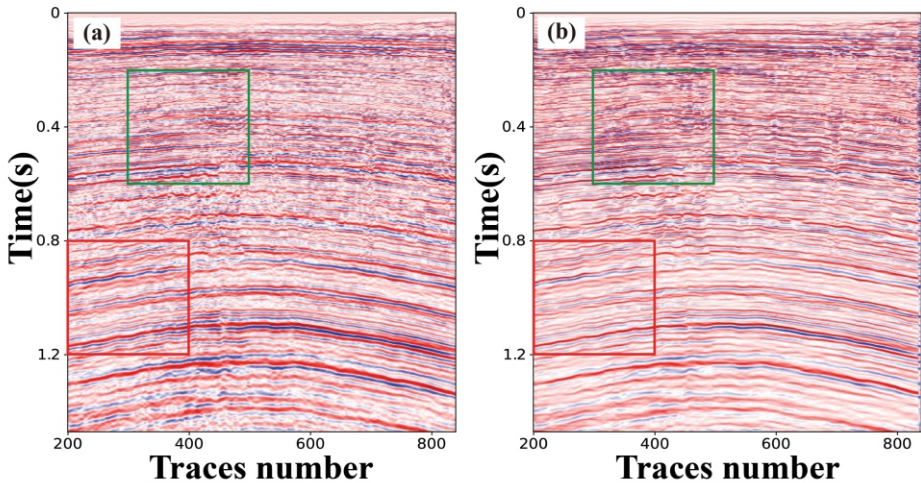
Fig. 12. Field data.

Fig. 13. Experimental results of proposed method on field seismic data. (a) Actual low-frequency data and (b) corresponding network output results.

Fig. 14 corresponds to the data in the green and red rectangles in Fig. 13, respectively. More details can be clearly observed from the enlarged display. Some difficult to distinguish thin layer structures in the data before processing are identified after processing, among which the parts marked by arrows are some thin layer structures identified by the model, and the longitudinal resolution of seismic data is significantly improved. The test on the field data demonstrates that, despite the obvious differences between the field data's frequency band range and signal-to-noise ratio and the training

data's, the training model still clearly enhances the frequency of the field data. This shows that the training model has a reliable generalization ability and can be applied to the frequency enhancing of the field data.
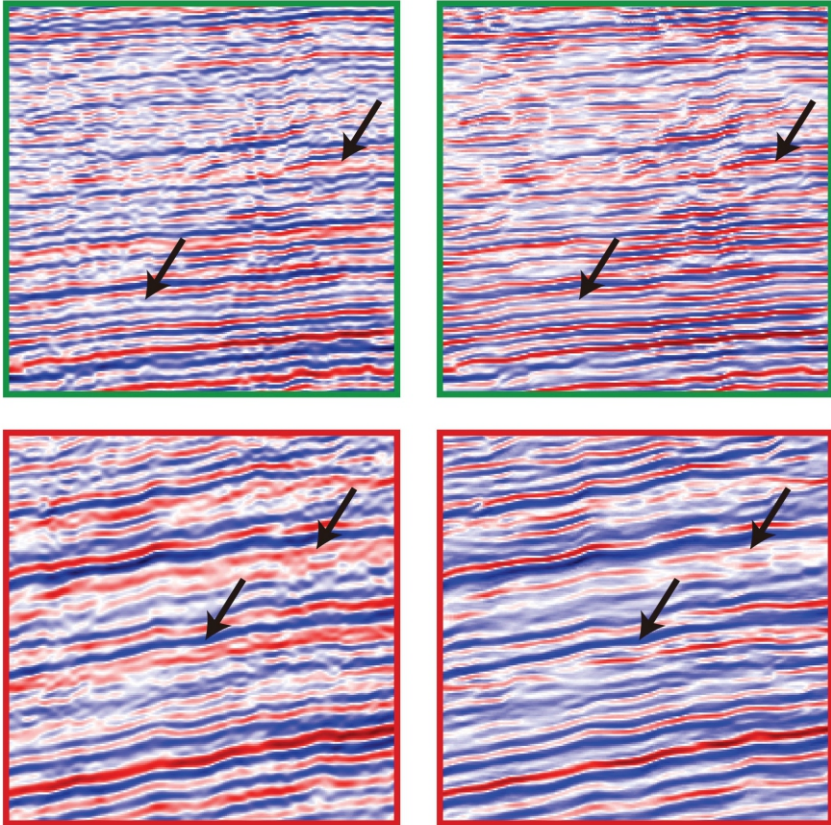

Fig. 14. Detail comparison of red and green boxes. (The left side is the actual data; the right is the network output data).

We performed a spectrum analysis using the Fourier transform on the field data and model output data to further demonstrate how the method improved the resolution of seismic data, as shown in Fig. 15. The amplitude spectrum of field data is represented by the blue curve, the amplitude spectrum of model output data are represented by the red curve, and the source of the enhancement of the high-frequency component is shown by the green arrow. By comparing the amplitude spectrum, we find the trained network enhances the upper cut-off frequency while retaining the low-frequency signal, effectively broaden the frequency width of the seismic data, and obviously recovers the high-frequency signal above 50 Hz, enhancing the main frequency of the seismic data from 36 Hz to 50 Hz.
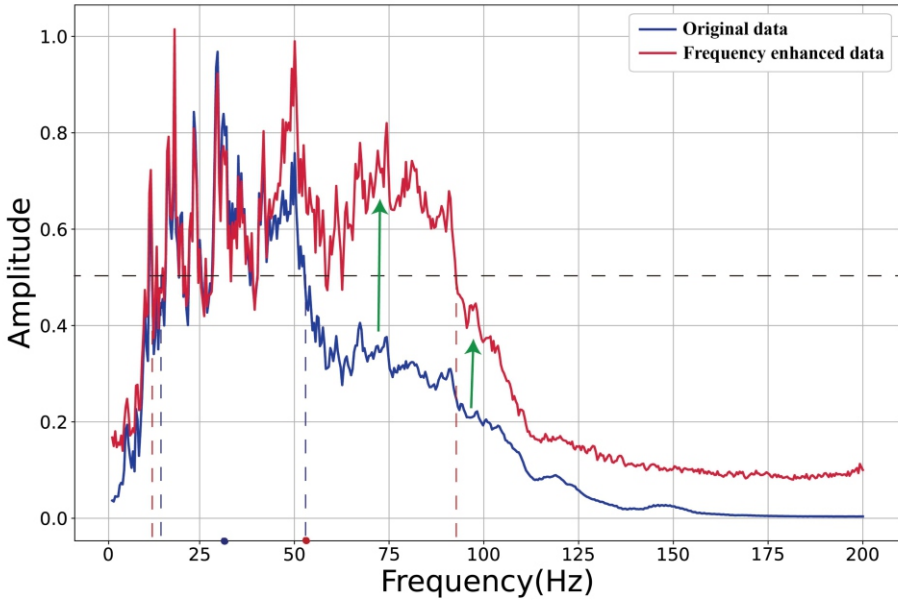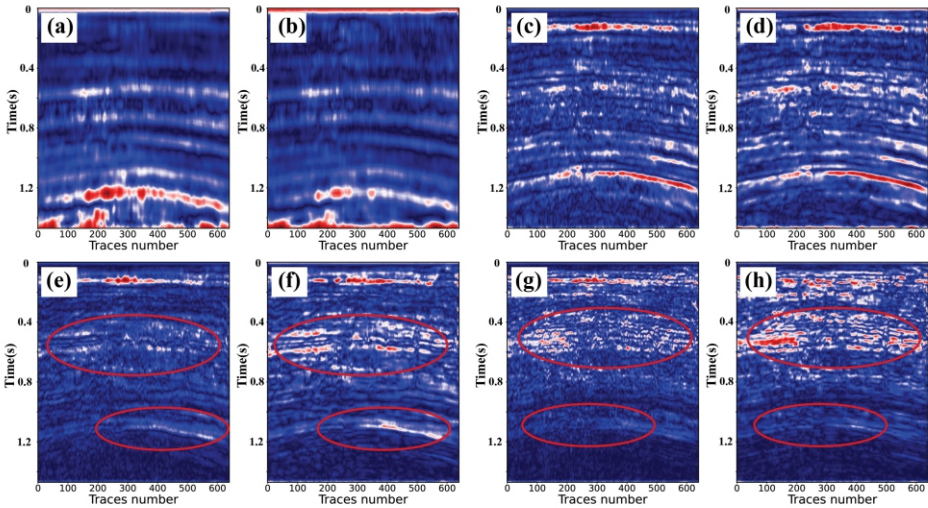
Fig. 15. Spectrum analysis of field data.

Fig. 16. Comparison of time-frequency decomposed seismic section. (a, c, e and g are the frequency division profiles of the field data; b, d, f and h are the frequency division profiles after processing; a and b are 20 Hz single frequency profiles; c and d are 40 Hz single frequency profiles; e and f are 60 Hz single frequency profiles; g and h are 80 Hz single frequency profiles).

We implement frequency division of seismic data using wavelet transform. Fig. 16 shows the frequency division profiles of original data and data after processing, corresponding to single frequency profiles of 20 Hz, 40 Hz, 60 Hz and 80 Hz, respectively. By comparing single-frequency profile data, it is easy to notice that most of the original low-frequency components between 20 Hz and 40 Hz are still present, and the high-frequency components between 60 Hz and 80 Hz are obviously recovered, as shown in the red circle in Figs. 16e-h. The results demonstrated that while the low-frequency component is completely retained, the recovery of high-frequency components from 60 Hz to 80 Hz is obvious, and the recovered high-frequency components are wholly consistent with the fine structure of the seismic data.

The main frequency of the whole data is raised and the bandwidth is enlarged, which verifies that the network trained by the synthetic data can also play the role of frequency raising for the field data.

CONCLUSIONS

By establishing a deep learning network based on a pre-training strategy, we proposed a high-resolution seismic data processing method. This strategy improves the model's data mining effectiveness and capability, and enables networks with specific capabilities to learn the mapping between the Ricker wavelet and wideband wavelet. To enable the constant improvement of network performance in training, the *ResPath* is simultaneously introduced into Res-Unet. Moreover, the loss function uses the weighted MS-SSIM and MAE combination.

The proposed deep learning method can successfully retain the low frequency signal while enhancing the main frequency and frequency band width of seismic data, according to the field data application. Moreover, the results of high-precision time-frequency analysis show that the elevated high-frequency components are based on evidence. Specifically, the source of the high-frequency components of the signal can be seen in the amplitude spectrum. The proposed method successfully recovers the high-frequency components in the frequency division profile, and the results are consistent with the geological structure, demonstrating that our method may successfully increase the vertical resolution of seismic data.

However, the method still has some limitations. The detailed geological structure that the model in this paper recovered may not be accurate (particularly in the areas with poor data quality). In subsequent studies, we can add well control to tune the parameters for better results. Additionally, different from image processing, the quality of seismic signals decreases with depth due to attenuation or absorption problems, therefore applying deep learning to geophysics would often have different effects in the shallow layer and deep layer. To achieve the same frequency enhancing effect in deep and shallow layers, we will consider using different loss functions for different depths or conducting separate training for different time intervals in the follow-up research of deep learning on geophysics.

ACKNOWLEDGMENTS

REFERENCES

Braga, I.L.S. and Moraes, F.S., 2013. High-resolution gathers by inverse Q-filtering in the wavelet domain. Geophysics, 78(2), 53-61.

Canning, A., Moulière-Reiser, D., Weiss, Y., Malkin, A., Phillip, E., Grinberg, N., Teitel, A., Reznikov, M. and Yehezkel, V., 2017. Neural networks approach to spectral enhancement. Expanded Abstr., 87th Ann. Internat. SEG Mtg., Houston: 4283-4286.

Chen, S. and Wang, Y., 2018. Seismic resolution enhancement by frequency-dependent wavelet scaling. IEEE Geosci. Remote Sens. Lett., 15: 654-658.

Chen, S., Wei, Q., Liu, L. and Li, X., 2018. Data-driven attenuation compensation via a shaping regularization scheme. IEEE Geosci. Remote Sens. Lett., 15: 1667-1671.

Choi, Y., Seol, S.J. and Jo, Y., 2021. Deep learning spectral enhancement considering features of seismic field data. Geophysics, 86(5): V389-V408.

Deng, M., Jia, R. and Tian, Y., 2020. Super-resolution reconstruction of seismic profile images based on deep learning. Comput. Engineer. Design (in Chinese), 41: 2332-2337.

Dong, C., He, K., Loy, C.C. and Tang, X,. 2015. Image super-resolution using deep convolutional networks. IEEE Transact. Pattern Analys. Mach. Intellig., 38: 295-307.

Gao. H., Liu, G. and Wu, X., 2021. ChannelSeg3D: Channel simulation and deep learning for channel interpretation in 3D seismic images. Geophysics, 86(4): IM73-IM83.

Halpert, A.D., 2018. Deep learning-enabled seismic image enhancement. Expanded Abstr., 88th Ann. Internat. SEG Mtg., Anaheim: 2081-2085.

He, K., Ren, S., Zhang, X. and Sun, J., 2016. Deep Residual Learning for Image Recognition. IEEE Conf. Comput. Vis. Pattern Recognit. (CVPR): 770-778.

Ibtehaz, N. and Rahman, M.S., 2019. MultiResUNet: Rethinking the U-Net Architecture for Multimodal Biomedical Image Segmentation. Neural Netw.. 121: 74-87.

Ioffe, S. and Szegedy, C., 2015. Batch normalization: accelerating deep network training by reducing internal covariate shift. Proc. 32nd Internat. Conf. Machine Learn. - Vol. 37 (ICML'15). JMLR.org, 448-456.

Jervis, M., Liu, M. and Smith, R., 2021. Deep learning network optimization and hyperparameter tuning for seismic lithofacies classification. The Leading Edge, 40: 514-523.

Kazemeini, S.H., Juhlin, C., Yang, C., et al., 2010. Enhancing seismic data resolution using the prestack bluing technique: An example from the Ketzin CO2 injection site , Germany. Geophysics, 75(6): V101-V110.

LeCun, Y., Bengio, Y. and Hinton, G., 2015. Deep learning. Nature, 521: 436-444.

Ledig, C., Huszar, F., Theis, L., et al., 2017. Photo-realistic single image super-resolution using a generative adversarial network. IEEE Conf. Comput. Vis. Patt. Recogn. (CVPR), 105-114.

Li, J., Wu, X. and Hu, Z., 2020. Deep learning for simultaneous seismic image super-resolution and denoising. Expanded Abstr., 90th Ann. Internat. SEG Mtg., Houston: 1661-1665.

Li, Q., 1994. The road to accurate exploration: Engineering analysis of high-resolution seismic exploration system. Petroleum Industry Press, Houston, TX.

Long, J., Darrell. T. and Shelhamer, E., 2015. Fully convolutional networks for semantic segmentation. IEEE Transact. Patt. Analys. Machine Intellig., 39: 640-651.

Margrave, G.F., Hrnley, D.C. and Lamoureux, M.P., 2011. Gabor deconvolution: esti-
mating reflectivity by nonstationary deconvolution of seismic data. Geophysics,
76(3): W15-W30.

Oliveira, D.A.B., Ferreira, R.S., Silva, R. and Brazil, E.V., 2019. Improving seismic data
resolution with deep generative networks. IEEE Geosci. Remote Sens. Lett.: 1-5.

Picetti, F., Lipari, V., Bestagini, P. and Tubaro, S., 2018. A generative adversarial net-
work for seismic imaging applications. Expanded Abstr., 88 th Ann. Internat. SEG
Mtg., Anaheim: 2231-2235.

Robinson, E.A. and Treitel, S., 1967. Principles of digital Wiener filtering. Geophys.
Prosp., 15: 311-332 .

Ronneberger, O., Brox, T. and Fischer, P., 2015. U-Net: Convolutional Networks for
Biomedical Image Segmentation. Internat. Conf. Medical Image Comput.-Assisted
Intervention. Springer Verlag, Berlin, 234-241.

Sun, Y., Yu, W. and Huang, Y., 2021. High resolution end-to-end seismic processing
technology based on U-NET network. Progr. Geophys. (in Chinese), 36:1297-1305.

Wu, X., Liang L., Shi, Y. and Fomel, S., 2019. FaultSeg3D: Using synthetic data sets to
train an end-to-end convolutional neural network for 3D seismic fault segmentation.
Geophysics, 84(3): IM35-IM45.

Xiao, X., Lian, S., Luo, Z. and Li, S., 2018. Weighted Res-Unet for High-Quality Retina
Vessel Segmentation. 9th Internat. Conf. Informat. Technol. Medicine Education
(ITME): 327-331.

Yan, Z., Fang, G., Xu, H.. Liu, J., Shi, J., Pan, J. and Wang, J., 2018. The application of
Hilbert spectral whitening method to high resolution processing of marine seismic
data. Marine Geol. Quatern. Geol., 38: 212-220.

Yuan, Z., Huang, H. and Jiang, Y., 2019. An enhanced fault-detection method based on
adaptive spectral decomposition and super-resolution deep learning. Interpretation.
7(3): 1-63.

Yu, S., 1996. Broadband Ricker wavelet. Oil Geophys. Prosp. (in Chinese), 5:
605-615+750.

Yu, S., Ma, J. and Wang, W., 2019. Deep learning for denoising. Geophysics, 84(6):
V333-V350.

Zhao, H., Gallo, O., Frosio, I. and Kautz, J., 2016. Loss functions for image restoration
with neural networks. IEEE Transact. Computat. Imag., **3**: 47-57.

Zhang, J., Zhang, B., Zhang, Z., Liang, H. and Ge, D. 2015. Low-frequency data analysis
and expansion. Appl. Geophys., 12: 212-220.